Extensive Loss and Gain of Conserved Non-Coding Elements during Early Teleost Evolution

Elisavet Iliopoulou* [1,2], Vasileios Papadogiannis* [1], Costas S. Tsigenopoulos[1], Tereza Manousaki[1]

1 Hellenic Centre for Marine Research (HCMR), Institute of Marine Biology, Biotechnology & Aquaculture (IMBBC)
2 CURRENT ADDRESS : Université de Paris, Centre National de la Recherche Scientifique, Institut Jacques Monod, Paris, France

* Authors contributed equally towards the analysis carried out and manuscript preparation.

Abstract

Conserved Non-coding Elements (CNE) in vertebrates are enriched around transcription factor loci associated with development, often participating in their regulation. However, loss and rapid divergence of CNEs has been reported in teleost fish, albeit taking only few genomes into consideration. Taking advantage of the vast increase in high-quality teleost genomes, we focus on identifying and studying the evolution of teleost CNEs. We carry out targeted genomic alignments and comparisons within the teleost phylogeny to detect CNEs and reconstruct the ancestral teleost CNE repertoire. Through this teleost-centric approach, not only do we confirm previous observations of extensive vertebrate CNE loss early in teleost evolution, but we also report massive CNE gain in the teleost stem-group over 300 million years ago. While kept vertebrate CNEs have signatures of slower evolution compared to newly gained CNEs, both groups of elements share highly similar characteristics. Using synteny-based gene association to link CNEs to putative targets, we show that the majority of teleost gained CNEs are found in the vicinity of orthologous loci involved in transcriptional regulation and embryonic development that are also associated with ancestral CNEs in other vertebrates. Moreover, teleost and vertebrate CNEs share a highly similar transcription factor binding site vocabulary dominated by homeobox, FOX, EST-related and bHLH binding motifs. Based on these data we suggest that early teleost CNE gains may reflect a restructuring of the ancestral CNE repertoire through both extreme divergence and de-novo emergence. Finally, we also show that newly identified pan-teleost CNEs have potential for accurate resolution of teleost phylogenetic placements in par with coding sequences, unlike ancestral only elements shared with spotted gar. Overall, this work provides new insight into CNE evolution, while offering a set of conserved putative regulatory elements with great value for follow-up work on phylogenomics, comparative genomics and the study of gene regulation evolution in teleosts.

Keywords: *CNE, Whole Genome Duplication, enhancer evolution, teleost comparative genomics, vertebrate comparative genomics*

Introduction

During embryonic development, the interaction of a network of Transcription Factors (TFs) with a variety of cis-regulatory elements found mainly in non-coding sequence drives the spatial and temporal regulation of gene expression with great precision[1]. In vertebrates, regulatory elements can be close to target genes (< 50kB) or even embedded in intronic areas, but many cis-regulatory modules are located from hundreds of kB to more than 1 Mb away[2]. Among the non-coding genome, a large number of vertebrate CNEs have maintained greater than 70% sequence identity for over 400 millions of years, exhibiting even greater average conservation than protein-coding genes[3]. Many of these CNEs act as enhancers for neighbouring genes associated with evolutionarily conserved functions, including important developmental processes[4]. While most vertebrate CNEs are found in a single copy in the genome, some CNE duplications have also been identified in paralogous genetic loci produced by the two rounds (2R event) of Whole Genome Duplication (WGD) that happened early in vertebrate evolution, suggested to have contributed to the diversification of the subphylum [5].

While jawed vertebrates share thousands of CNEs, a few hundred of these elements, including duplicate CNEs, are even conserved with lamprey, a member of the basally splitting jawless vertebrates[6]. Therefore, the evolution of a set of ancestral vertebrate CNEs predates the split of jawless and jawed vertebrates, possibly dating to the first WGD shared by both lineages, with additional CNEs established after the second WGD of jawed vertebrates. Within vertebrates, teleost fish form the most species-rich monophyletic group. It is hypothesized that one of the main drivers of their widespread diversification is the teleost-specific (3R event) WGD[7]. Because of 3R, teleost genomes carry additional paralog genes that has led to increased genetic diversity. Unexpectedly, in contrast to gene coding regions, previous studies have suggested extensive loss and rapid divergence of ancestral vertebrate CNEs following the 3R WGD event[7,8], though this has been based on few model species and based on comparisons to other vertebrates. To date, the drivers of this massive loss of CNEs after 3R have been unexplored, while the conservation of non-coding elements within the teleost clade has remained uncharacterized.

Previous studies on teleost CNE evolution had mainly focused on the fate of ancestral vertebrate CNE in teleost fish[9]. Therefore, a comprehensive catalogue of non-coding elements conserved within the teleost group has been lacking and how the CNE landscape responded to the 3R WGD has remained unresolved. Here, we focus on identifying and studying teleost CNEs through a teleost-centric search, with the main focus of investigating the evolution of CNEs following the 3R WGD. For this purpose, we first carry out targeted genome alignments of key focal species and then use these data to detect CNEs across the teleost phylogeny. Drawing information of CNE presence and absence in different teleost groups, we reconstruct the ancestral teleost CNE repertoire and carry out comparisons to ancestral vertebrate CNEs, using the spotted gar as an outgroup species predating the 3R. Using this dataset, we are able to confirm massive CNE loss in the teleost lineage, but we also report extensive CNE gain following 3R, that largely compensates for lost elements. Focusing on single copy CNEs with presence in all teleost taxa in our dataset, we find pan-

teleost CNEs have comparable potential to gene sequence for accurately resolving phylogenetic placements, unlike previously described ancestral only elements shared with spotted gar. We assess evolutionary signatures and synteny conservation of teleost CNEs and use an orthology-guided synteny-based approach to associate CNE gains and losses with candidate conserved gene targets with putative regulatory links to studied CNEs, finding that the majority of gained CNEs are near loci that are orthologous to CNE associated genes in other vertebrates. Finally, we show that the majority of both gained and ancestral CNEs share highly similar profiles of transcription factor binding site composition. Taken together our data support that teleost gained CNEs may include cases of extreme sequence divergence, working in concert with *de novo* CNE birth. This work represents the first CNE analysis on a large number of teleost genomes and as such it provides unique insight for understanding the evolution of the conserved noncoding genome of teleosts.

Materials and Methods

All analyses were carried out on the Zorbas HPC infrastructure of IMBBC – HCMR [10].
To identify teleost CNEs we used the identification pipeline described below and presented in Supplementary Figure 1. Briefly, we first selected 24 teleost genomes and the spotted gar genome from the Ensembl database, aiming for high contiguity (N50 > 8Mb), high completeness (BUSCO score of > 95%) and broad sampling across the teleost phylogeny. We then used pairwise whole genome alignments from two selected pairs of focal reference species for de novo CNE identification and used these starting CNE sets to identify ancestral teleost elements, as well as CNE gains and losses across the phylogeny.

CNE Identification pipeline

Pairwise whole-genome alignment

We performed pairwise reciprocal whole-genome alignments with LASTZ v1.04.03 [11] for two focal reference pairs of genomes downloaded from the Ensembl database[12], *Danio rerio* (Zebrafish - DanRer11) VS *Astyanax mexicanus* (Mexica tetra - Astyanax_mexicanus-2.0) and *Takifugu rubripes* (Fugu - fTakRub1.2) VS *Sparus aurata* (Gilthead seabream - fSpaAur1.2). These pairs were selected as representatives of the two most basally splitting clades of teleost phylogeny (206 - 252 MYA [13]), to allow for inference of ancestral CNE sets through comparisons across the phylogeny. All genomes were downloaded hard masked, i.e., interspersed repeats and low complexity regions were detected with the RepeatMasker tool[14] and were replaced with Ns. To conduct the alignments, we split input genomes in 10Mb windows with 100kb overlaps for Zebrafish and Fugu and non-overlapping 10Mb windows for Mexican tetra and Gilthead seabream. Two rounds of pairwise whole-genome alignments were run for each pair as discussed by Hiller *et al* 2013 [15]. In the first round, we used the following more sensitive LASTZ parameterization recommended for distantly related species (> 100 Mya): M=50 E=30 H=2000 K=2200 L=6000 O=400 T=1 Y=3400 Q=HoxD55.q [16]. Subsequently, a second round of alignment was performed after masking aligned regions from the first alignment round, to facilitate the identification of conserved

elements not found in the initial alignment. During the second round, the following less sensitive LASTZ parameters were used: K=1500, L=2300, M=0 and W=5 [15].

Chaining - Netting

Aligned regions found by the two rounds of pairwise whole-genome alignment were chained using the CNEr v1.8.3 Bioconductor wrapper functions[16] inside an R environment (using utilities found in UCSC Browser [17]). During chaining, matching initial alignments that are sufficiently close are joined into bigger alignment chains, with the longest fragments further connected to form netted alignments in net Axt format (Supplementary figure 1).

CNE Identification in reference focal species

Alignment chain nets from the two focal reference pairs (Zebrafish VS Mexican tetra and Fugu VS Gilthead seabream) were used for *de novo* CNE identification using Zebrafish and Fugu as reference genomes. Exonic regions were filtered out of alignments, using gene annotation information from the Ensembl database (*Takifugu_rubripes.fTakRub1.2.104 , GCF_900880675.1_fSpaAur1.1_genomic, Astyanax_mexicanus-2.0.104*, *Danio_rerio.GRCz11.104*). The CNEr v1.28.0 Bioconductor package[16] was used for both filtering and CNE detection. Conserved regions were selected based using the following parameters: 1) A maximum number of 4 hits per element (cutoffs = 4), i.e., how many times we expect to see an element. 2) A minimum identity of 70% for aligned regions (Identities = 70pc), i.e., the minimum percentage of matches in a single alignment and 3) A sliding window size of 100bp for detection (windows = 100).

Positive control and comparison with published data

While optimizing the parameterization of our CNE identification pipeline, we aimed to achieve at least 95% recovery of previously identified highly conserved ancestral CNE shared among teleosts and other vertebrates, comparing our Zebrafish-Mexican tetra chained alignments against publicly available Zebrafish-Human pairwise genome alignment chains downloaded from the UCSC Genome Browser or comparing our zCNE dataset against Zebrafish-Mexican tetra CNE for a published Zebrafish CNE dataset (using danRer7) [15] derived from the comparison of Zebrafish with 15 other vertebrate genomes, including four teleosts, as well as a zebrafish CNE dataset (using danRer10) from the ANCORA database[18].

CNE search in other teleost species

Using the *de novo* identified CNE datasets from Zebrafish (*zCNEs*) and Fugu (*fCNEs*), we searched 20 other teleost fish genomes pre-masked for repeats via BLAST v2.10.0+ [19] for zCNE and fCNE presence / absence (evalue <= $1e^{-06}$, word size=6, max target seqs=1, max hsps=1). This comparative dataset (Supplementary table 1) was used as the basis for studying CNE conservation, gain and loss, as well as CNE based phylogenomic analyses.

CNE-based phylogenomic analysis

For CNE-based phylogenomic reconstructions we used single copy CNEs shared by all species in the phylogeny, including or excluding spotted gar (*Lepisosteus oculatus*) as an outgroup species belonging to the Holostei infraclass of ray-finned bony fish, which diverged before the 3R WGD [20]. To extract CNE sequences for multiple alignments from different

teleost or spotted gar, we used BLAST derived coordinates extended by 50bp in either side to maximize alignable sequence capture (Supplementary Figure 2). Multiple sequence alignments were carried out using MAFFT v7.407 [21] and CNE alignments were collated with custom bash scripting to produce a single supermatrix of all CNE from across all species in each phylogeny. TrimAl v1.4.rev15 [22] was used for alignment trimming with a gap threshold of 50% of (gt 0.5). RAxML-NG v.1.0.2 [23] was used for CNE-based tree construction using 20 starting trees (10 parsimony + 10 random) and 100 bootstraps, with TVM+I+G4 selected as the best-fit model with ModelTest-NG[24]. For visualization purposes FigTree v1.4.4 [25,26] was used. Gene-based reconstruction was carried out with the same pipeline, using single copy orthologous proteins for all species included predicted by OrthoFinder2 v2.5.4 [27] from the proteomes of these species. Protein sequences were aligned with MAFFT v7.407, collated to a supermatrix with subsequent trimming using TrimAL v1.4.rev15 (gt 0.5) and tree construction with RAxML-NG v.1.0.2 using 20 starting trees (10 parsimony + 10 random) and 100 bootstraps, with JTT+I+G4+F selected as the best-fit model with ModelTest-NG.

Identifying the vertebrate CNE set

For inference of ancestral vertebrate CNE losses in teleosts, CNE datasets for *Homo sapiens* (Human), *Callorhinchus milii* (Elephant shark) and *Lepisosteus oculatus* (Spotted gar) (using Human as reference) were downloaded from the ANCORA database and were re-filtered for coding regions (*H. sapiens* gene predictions from RefSeq, Genbank, CCDS, UniProt and the UCSC KnownGene track), selecting sequences with >70% identity over a window of 100 bases. These ancestral vertebrate CNE were then searched in the 24 teleost genomes in the study using BLAST (evalue=1e-6, word size=6, max target seqs=1, max hsps=1).

Ancestral teleost CNEs Identification and Categorization

We based our ancestral CNE identification protocol on comparisons between the two earliest splitting teleost clades in our phylogeny hereby defined as: Clade 1 (highlighted in orange in Figure 2A) spanning from *Siluriformes* represented by *P.hypophthalmus* to *Cypriniformes* represented by *D.rerio* and Clade 2 (highlighted in blue in Figure 2A) spanning from *Cyprinodontiformes* represented by *K.marmoratus* to *Tetraodontiformes represented by M.mola.* To infer the ancestral teleost CNE set (from now on abbreviated as atCNEs), we selected zCNEs with presence in any clade 2 species and fCNEs not overlapping zCNEs with presence in any clade 1 species.

We then searched for atCNEs presence in spotted gar or other vertebrates (ghost shark, western clawed frog, chicken, green anole and human) via BLAST (evalue=1e-6, word size=6, max target seqs=1, max hsps=1) and allocated atCNEs to the following categories based on their inferred time of origin: 1) Elements identified in any vertebrate other than spotted gar were categorized as ‘vertebrate atCNEs’, inferred to be ancestral to ray-finned fishes, 2) Elements present in spotted gar and absent from all other vertebrates were categorized as ‘neopterygian atCNEs’, inferred to have been gained in the common neopterygian ancestor with spotted gar, 3) Elements present only in teleosts were categorized as ‘3R atCNEs’, inferred to have been gained in the teleost common ancestor.

CNE distribution / localization over zebrafish chromosomes for Figure 1B was plotted using Circos [28] and for Figure 6 using Rideogram [29].

CNE Sequence and Synteny Conservation Analyses

To calculate CNE sequence conservation scores in three representative genomes from different parts of the phylogeny (*D. rerio*, *O. niloticus* and *T. rubripes)*, we carried out multiple whole genome alignments for all 25 species in the study with CACTUS (v 2.2.1) [30], applied phyloFit [31] for phylogenetic model fitting (using the REV substitution model) for each chromosome for each species and then used phyloP [32] to infer base-wise conservation scores (SPH method, CONACC mode). We then calculated average phyloP (CONACC) scores for zCNEs present in each species, as well as exonic areas, and plotted conservation scores over the 25 zebrafish chromosomes as a heatmap using Circos [28]. CNE synteny plotting for Figure 3 was created using the JCVI MCscan pipeline [33].

Gene association and Ontology Enrichment

The association of CNEs with putative gene targets was carried out through an orthology-guided synteny-based approach. First, we extracted all genes that lie within a 1Mb window of each CNE in each teleost species. A synteny score was attributed to each CNE - gene pair for zCNEs (Zebrafish as reference), fCNEs (Fugu as reference) or vCNEs (human as reference) which corresponds to the number of species in which the CNE is proximal to an orthologous gene, based on orthology information for all genes across species obtained by OrthoFinder2 v2.5.4. We then calculated a proximity rank for each target gene, which corresponds to the average position of a gene relative to a CNE, when all proximal genes are ordered in increasing distance (Figure 4A). CNEs were associated with candidate target genes with the highest synteny score (cutoff threshold of at least 5 species) and the lowest proximity rank (accepting all ties with the same syntenic score). Associated atCNE targets in zebrafish or Fugu were then compared to associated vCNE targets in human, using Orthogroup information from OrthoFinder2. Gene targets of atCNE with orthologous loci associated with vCNE were annotated as “ancestral targets” and gene targets without orthologous loci associated with vCNE were annotated as “novel targets”. Furthermore, we used a bootstrap resampling approach to obtain support that the observed levels of association with ancestral targets were non-random. zCNEs or fCNEs were randomly associated with subsets of genes sampled from all zebrafish or Fugu genes which were compared to vCNE associated loci and the total number of ancestral or novel target associated CNE was counted. Using 10,000 bootstrap replicates with different random subsets, we calculated the average count, standard deviation and z score for ancestral or novel target associated elements and obtained strong support (z score <= 22) that associations were non-random. Gene ontology enrichment for GO biological process terms in different associated target gene sets was carried out through gProfiler [34].

CNE Paralog Analysis

To identify CNE paralogs and clusters of paralogous CNE loci, we first carried out self-BLAST searches for zebrafish atCNEs and Fugu atCNEs to identify elements in each dataset with non-self hits. Gene paralog information for each species was then acquired from the Ensembl database and used to annotate putatively paralogous atCNE loci (as inferred from BLAST matches) based on the paralogy of their associated target genes. Gene paralog information was also used to infer the origin of paralogous atCNE loci prior or

after the 3R WGD, based on the clade of origin of paralogous genes. In parallel, the same pipeline was applied to human vCNEs and paralogous vCNEs were then compared to paralogous atCNEs to identify shared / orthologous paralogy clusters between the two groups.

Motif Prediction and Transcription Factor Binding Site Enrichment

De novo motif prediction and transcription factor binding site enrichment analysis for different CNE sets were carried out using XSTREME online from the MEME suite. Enriched TFBS were grouped to higher order categories based on similarity inferred from their consensus motifs and XSTREME motif clustering information. We also carried the same enrichment analysis on a subset of 10,932 random non-CNE zebrafish 24hpf embryonic enhancers downloaded from the EnhancerAtlas 2.0 database[35] with comparable size distribution to CNE sets.

Results

Teleost CNE identification and ancestral set reconstruction

First, we carried out whole-genome pairwise alignments in two pairs of focal reference species with high-quality annotations in selected positions of the phylogeny: 1) Zebrafish VS Mexican tetra and 2) Fugu VS Gilthead seabream. After filtering out coding and repetitive regions, this investigation resulted in a set of 298,743 conserved sequence chains between Zebrafish and Mexican tetra and 372,053 chains between Fugu and Gilthead seabream, yielding a total of 63,023 Zebrafish-Tetra CNEs (zCNE) and 39,532 Fugu-Seabream CNEs (fCNE) of at least 100bp with >=70% sequence identity.

We used the zCNE and fCNE datasets as reference CNE queries to scan the other teleost genomes via BLAST, while we also included the spotted gar genome as an outgroup to identify CNE gains and losses following the 3R WGD. BLAST results are presented in Supplementary table 2. This approach allowed us to infer the ancestral teleost CNE set, by using presence/absence information of zCNEs and fCNEs in different species of our phylogeny. Taking advantage of the phylogenetic positions of our selected focal species, we carried out a bidirectional comparison, reviewing the presence of fCNE in the Zebrafish-tetra clade (Clade 1) and the presence of zCNE in the Fugu-Seabream clade (Clade 2), as described in more detail in the methods and summarized in Figure1A. This search identified 7,358 fCNEs present in at least one species of Clade 1 and 22,596 zCNEs present in at least one species of Clade 2. Combining these sets produced a final set of 25,930 non-overlapping unique elements that consists the ensemble of CNEs inherited by at least two or more species in our phylogeny from the teleost common ancestor (atCNEs).

Extensive CNE gain and loss during early teleost evolution

The reconstruction of the atCNE set offered us the chance to not only review previously demonstrated CNE loss in teleosts, but also assess putative gains during early teleost evolution. For this purpose, we used similarity searches to find which atCNEs have hits in spotted gar and any of five other vertebrate genomes (ghost shark, western clawed frog, chicken, green anole and human). In this way, we identified 6,585 atCNE that are also found in other vertebrates (Vertebrate atCNE), 6,934 atCNE that are shared only with spotted gar and no other vertebrates (Neopterygian atCNE) and 12,411 atCNE with no hit in vertebrates or spotted gar and are teleost specific (3R atCNE) (Figure1A). We also used publicly available sets of CNE from the ANCORA database, combining non-overlapping unique CNE shared by human-spotted gar and human-ghost shark to obtain an Ancestral Vertebrate CNE set (vCNEs). Searching for vCNEs in any of the teleost genomes in our phylogeny confirmed previously reported levels of loss of ancestral vCNEs in teleosts (69.5%) (Figure1A). However, our teleost-centered approach for CNE identification revealed that this loss of ancestral CNE in teleosts was accompanied by extensive gain of new elements. While a large number of new CNEs (35.8%) were gained in the neopterygian ancestor, the majority of new elements (64.2%) were acquired after the split with spotted gar, following the 3R WGD.

Vertebrate CNEs are known to be distributed non-randomly in the genome, with many clustering around developmental transcription factor genes. To assess if gained atCNEs follow a similar distribution pattern, we looked into the distribution of the three different categories of atCNEs in the zebrafish genome. After dividing the zebrafish genome in 500kb non-overlapping windows (Hereby called 500kb Zones), we counted total CNE content for each category in each window and plotted CNE count as a heatmap, with each category plotted as homocentric circles (Figure1B). This search showed that the majority of Zones containing vertebrate atCNEs (89.2%) also contained gained CNEs, with 80.4% of neopterygian atCNEs and 84.7% of 3R atCNEs found in ancestral vertebrate zones. Respectively novel zones without vertebrate atCNEs have much lower total CNE content, with novel neopterygian zones (40.2% of all zones with neopterygian atCNEs) containing only 19.6% of all neopterygian atCNEs and novel 3R zones (30.9% of all zones with 3R atCNEs) containing only 15.3% of all 3R atCNEs. In addition, a quarter of the genome (25.6% - 682/1982 zones) was devoid of CNEs, supporting that all categories of teleost CNEs (whether ancestral or gained) are non-randomly distributed, comparable to other vertebrates.

The value of atCNEs as Phylogenetic Markers

Having obtained a comprehensive set of CNEs conserved across different teleosts, we used this opportunity to assess the potential of atCNEs as phylogenetic markers. We constructed two CNE based phylogenies, one with an extended dataset of 4673 pan-teleost atCNEs present in all teleost species in the study but excluding spotted gar and one from a subset of the pan-teleost dataset with 2668 elements also present in spotted gar. In parallel, we also constructed a protein-based phylogeny using universal single copy ortholog genes as a control for assessing resulting topologies from the CNE-based reconstructions. Use of the pan-teleost dataset of 4673 atCNEs lead to the recovery of the expected topology, as supported by the gene-based tree (supplementary Figure1), with maximal bootstrap support

for all clades (Figure2A). In contrast, the dataset including spotted gar resulted in topological discrepancies in the relationships of *Lates clalcarifer, Seriola dumerili* and *Scophthalmus maximus* and lower support in some of the clades (Figure2A).

Variable Ancestral CNE loss across the Teleost Phylogeny

While 4673 atCNEs (18%) were present in all taxa studied as mentioned, most atCNEs were missing in one or more species. To characterize patterns of atCNE gain and loss in different teleosts, we mapped rates of loss for each atCNE category as a percentage of all identified atCNEs, as presented in Figure2B. This revealed a range of CNE loss across the phylogeny, with different species having variable atCNE retention levels, irrespective to their phylogenetic position (Figure2B). In contrast, a clearer pattern of incremental loss was seen for different atCNE categories (Figure2B). Vertebrate atCNEs showed the lowest rates of loss ranging from 0.84% to 6.09%, with an average loss of 3.18% (standard deviation = 1.33%). In turn, neopterygian atCNEs showed nearly two-fold loss in comparison, ranging from 1.08% to 10.53%, with an average loss of 5.31% (standard deviation = 2.56%). Finally, 3R atCNEs accounted for two thirds (average 68.1%) of total atCNE loss, with their loss ranging from 3.67% to 28.75% of all atCNEs, with an average of 17.82% (standard deviation = 6.78%).

High Sequence and Synteny Conservation across teleost CNE

Vertebrate CNEs are characterized by high levels of sequence conservation, being on average more conserved than exonic areas[36]. To assess to what extent different categories of teleost CNEs follow this pattern of slow evolution, we carried out multiple whole genome alignment of the genomes included in our phylogeny and calculated phyloP conservation scores for CNEs in Zebrafish, Fugu and Nile Tilapia. We also assessed CNE synteny in chromosome level genomes included in our phylogeny, hypothesizing that the clustered distributional pattern of the majority of atCNEs around specific genomic regions suggested high synteny conservation.

Comparing the two groups of sequences, CNEs have clear clustered distribution, as shown earlier, distinct from the more homogeneous distribution of genic regions (Figure3A). In addition, not only are average CNE phyloP scores significantly higher than that of exonic sequences, but atCNE categories also differ in their average conservation scores. Vertebrate atCNEs have higher average phyloP scores than Neopterygian atCNEs, which in turn have higher phyloP scores than 3R atCNEs (Figure3B). CNE synteny is also largely conserved across teleosts, with larger syntenic areas shared among clade 2 species and notable rearrangements compared to zebrafish and spotted gar (Figure3C).

Gene Association and Paralog Analysis Highlight Teleost CNE Evolution

The high levels of CNE turnover in early teleosts, together with conserved synteny and clustered organization of teleost CNEs, prompted us to examine their genomic localization more closely. We hypothesized teleost CNEs, similar to vertebrate CNEs, would reside around loci involved in developmental functions, which was additionally supported by their comparable non-random distribution. Since CNEs have been shown to act as conserved developmental enhancers, we undertook a synteny based association approach to identify putative gene targets. (Figure 4A).

Our gene association pipeline was able to associate 20168 zCNEs with 4444 zebrafish genes and an additional 2790 fCNEs not corresponding to zCNEs with 1146 Fugu genes. Comparing these sets to vCNE associated genes in human revealed that 85.46% of all atCNEs with targets were associated with a locus that has a human ortholog located within 1MB of a vCNE. We termed these loci with human orthologs associated with vCNE "ancestral targets" and respectively termed loci without human orthologs associated with vCNEs "novel targets" (Figure 4B). Looking at individual categories of atCNE with targets, 92.08% of vertebrate atCNEs, 85.95% of Neopterygian atCNEs and 81.08% of 3R atCNEs were associated with ancestral targets (Figure 4B). Gene ontology enrichment for ancestral atCNE targets showed high enrichment for genes involved in transcriptional regulation, the development of various organ systems and neuronal specification (Table 1). Novel atCNE targets were mainly enriched for developmental processes already associated with ancestral target sets, but had significantly weaker enrichment support, while only one process (regulated exocytosis) was specifically enriched in novel target genes (Table 1).

Through our target association analysis, we noticed that many 3R WGD derived paralogous loci were proximal to atCNE. To identify WGD derived CNE copies, we combined self-BLAST searches of zebrafish and Fugu atCNE with paralogy information from ENSEMBL. In parallel, we also applied the same methodology to human vCNE and compared vCNE and atCNE paralogous loci to probe ancestral CNE fate after the 2R and 3R WGD. Our analysis identified 89 vCNE paralogy clusters in human and 202 atCNE paralogy clusters in zebrafish, with 33 common paralogy clusters shared by both groups (Figure 4C). Of the total 977 paralogous atCNEs, 69.3% are vertebrate atCNEs, 21.8% are Neopterygian atCNEs and 8.9% are 3R atCNEs (Figure 4C). A total of 215 atCNEs (22%) are located in ancestral (2R derived) paralog clusters, with the remaining majority of 762 atCNEs (78%) found in 3R derived paralog clusters (Figure 4C).

Gained and Ancestral Teleost CNE Share Similar Motif Vocabularies

The identification of a large number of neopterygian atCNEs provides evidence for the widespread *de-novo* birth of CNEs, as these elements are present in spotted gar, which does not share the extensive loss of ancestral CNEs seen in teleosts. However, the association of the majority of atCNEs with ancestral gene targets also suggested that 3R atCNEs may not solely correspond to novel elements, but they could also include ancestral elements that have diverged beyond recognition at the sequence level. To assess if gained atCNEs may be divergent ancestral elements, we carried out motif and transcription factor binding site (TFBS) enrichment on different sets of atCNEs (Vertebrate, Neopterygian, 3R) and vCNEs (Lost and Kept in Teleosts). In parallel, as a control, we also carried the same

enrichment analysis on 10,932 random non-CNE zebrafish enhancers with similar size distribution to our CNE sets. All CNE categories, but not non-CNE enhancers, were found to share a common TFBS vocabulary, dominated by the homeobox (40-60% of CNE), FOX (35%-61%), EST-related / C2H2 zinc finger (28%-47%) and bHLH (15%-33%) classes (Figure 5). De-novo motif discovery also found an enrichment for the "TAATTA" homeodomain binding motif, centrally positioned in 18%-24% of all CNEs (Figure 5). No shared enriched motifs were found between any atCNE and vCNE combinations, but 19.7%-53.3% of atCNEs contained Prdm5 sites, which were not enriched in vCNE (Figure 5). Additionally, 14.8% of 3R atCNEs contained PAX2 sites, which were not specifically enriched in any other CNE category.

Discussion

This work presents the first attempt to catalogue the previously undocumented variety of Neopterygian and teleost CNEs by using a teleost-centric identification protocol. This approach is able to achieve high levels of CNE identification with low to moderate time and resource requirements, combining thorough pairwise whole genome alignments for strategically selected focal species with faster BLAST scanning for a wider range of teleosts. This offers an attractive methodology for fast CNE searches in large genomic datasets, representing an efficient way for answering questions of ancestral CNE gains and losses. Our work also offers support on the value of CNEs as a tool for robust phylogenomic reconstruction of teleost relationships, drawing attention on the importance of appropriate outgroup selection, as in the case of spotted gar shared elements.

Properties of Teleost CNE

Importantly, key properties of teleost CNEs are elucidated here: 1) They are distributed over the similar overlapping genomic regions, regardless of their time of origin 2) They show high sequence and synteny conservation over large evolutionary distances, comparable to CNEs in other vertebrates [36,37] 3) They are syntenically associated with loci involved in development related processes and transcription factor genes 4) They are enriched for development related transcription factor binding sites, with many harboring homeodomain binding motifs centrally in their sequence. The latter characteristic is in line with previous reports of AT enrichment in the conservation core of vertebrate CNEs, suggested to emerge from an overrepresentation of homeodomain binding motifs[38,39].

The Evolutionary Dynamics that shaped the teleost CNE Repertoire

The massive loss of ancestral CNEs in Teleosts has consisted a mystery since early studies of vertebrate CNEs, mainly because intuition would suggest the expected impact of the 3R WGD to be an addition of new paralogous CNEs to existing elements incrementally. Consequently, finding that novel CNEs gained in stem-teleosts have highly similar characteristics as ancestral vertebrate elements is pivotal for advancing our understanding of CNE evolution. While possibly counter-intuitive at first, this re-establishment of the CNE

repertoire following the 3R WGD is comparable to the fixation of ancestral CNEs in the jawed vertebrate common ancestor. With only few hundreds of CNEs shared with lamprey and only tens of elements recognizable in amphioxus, the vast majority of vertebrate CNEs were fixed after the second WGD in jawed vertebrates[40]. CNE associated targets, as well as experimentally confirmed regulated targets, include loci involved in the development of the central and peripheral nervous systems, as well as heart and muscle during the specification of these tissues at the phylotypic stage[41]. However, most of the innovations related with these cell populations and their associated gene regulatory networks predate the split of jawed vertebrates and are shared with cyclostomes. Similarly, we observed that the majority of teleost gained CNEs are also associated with these ancestral targets involved in developmental regulation at the phylotypic stage. This is in contrast with younger clade specific CNE gains in mammals, which have been associated with novel target loci, many of which are involved in protein-binding [42,43]. Similarly, previous work showed that older vertebrate CNEs are implicated in transcriptional and developmental regulation, while younger mammalian elements are associated with genes involved in post-transcription modification[44]. Finally, gained (either Neopterygian or 3R) teleost CNE also share a highly similar motif and binding site composition as vertebrate CNE, supporting they are also regulated by similar upstream networks. Consequently, we hypothesize that the majority of gained CNEs in teleost represent a reconfiguration of the ancestral vertebrate CNE repertoire linked to the regulation of the same key ancestral targets, instead of components of a new network regulating teleost specific processes.

CNE Gain by Sequence Divergence and De Novo Emergence

While atCNE of different origin categories have largely comparable characteristics, there are differentiating features that are detected when comparing gained (Neopterygian or 3R) and ancestral (vertebrate) teleost CNE. When considered in decreasing age of conserved sequence fixation (Vertebrate > Neopterygian > 3R), older atCNEs show higher average conservation, have lower loss rates across the phylogeny and are associated with more ancestral target genes compared to newer elements. These differences likely originate from the minorities of neopterygian and 3R atCNEs that are located within novel genomic regions without vertebrate atCNE and which are associated with novel teleost specific targets (Figure 6A). Based on this deviating profile compared to other atCNEs, it can be suggested that these novel-target associated elements are cases of de novo CNE emergence, as part of teleost specific regulatory networks. We therefore hypothesize that the ensemble of the CNEs gained in the stem-teleost lineage derived from two complementary scenarios of evolutionary origin (Figure 6B). The homogeneous profile of the majority of atCNEs is compatible with a scenario of CNE gain through extreme sequence divergence, in which ancestral vertebrate elements deviate in primary sequence, while retaining ancestral TFBS content and remaining associated with ancestral targets. This must have then been coupled with de-novo gains, as supported by both the emergence of novel-target teleost specific elements and the evolution of Neopterygian CNEs around ancestral targets prior to the extensive CNE loss in teleosts.

Code Availability

All custom scripts used in this project will be made available through https://github.com/genomenerds/CNE_analysis.

References

1. [Eric_H._Davidson]_The_Regulatory_Genome_Gene_Reg(BookFi).
2. Jeong, Y., El-Jaick, K., Roessler, E., Muenke, M. & Epstein, D. J. A functional screen for sonic hedgehog regulatory elements across a 1 Mb interval identifies long-range ventral forebrain enhancers. *Development* **133**, 761–772 (2006).
3. Polychronopoulos, D., King, J. W. D., Nash, A. J., Tan, G. & Lenhard, B. Conserved non-coding elements: Developmental gene regulation meets genome organization. *Nucleic Acids Res* **45**, 12611–12624 (2017).
4. Woolfe, A. *et al.* Highly conserved non-coding sequences are associated with vertebrate development. *PLoS Biol* **3**, (2005).
5. Soukup, S. W. Evolution by gene duplication. S. Ohno. Springer-Verlag, New York. 1970. 160 pp. *Teratology* **9**, (1974).
6. Papadogiannis, V. *et al.* Hmx gene conservation identifies the origin of vertebrate cranial ganglia. *Nature* **605**, (2022).
7. Glasauer, S. M. K. & Neuhauss, S. C. F. Whole-genome duplication in teleost fishes and its evolutionary consequences. *Molecular Genetics and Genomics* **289**, 1045–1060 (2014).
8. Lee, A. P., Kerk, S. Y., Tan, Y. Y., Brenner, S. & Venkatesh, B. Ancient Vertebrate Conserved Noncoding Elements Have Been Evolving Rapidly in Teleost Fishes. *Mol Biol Evol* **28**, 1205–1215 (2011).
9. Lee, A. P., Kerk, S. Y., Tan, Y. Y., Brenner, S. & Venkatesh, B. Ancient Vertebrate Conserved Noncoding Elements Have Been Evolving Rapidly in Teleost Fishes. *Mol Biol Evol* **28**, 1205–1215 (2011).
10. Zafeiropoulos, H. *et al.* 0s and 1s in marine molecular research: A regional HPC perspective. *Gigascience* **10**, 1–12 (2021).
11. rsharris_phd_thesis_2007.
12. Howe, K. L. *et al.* Ensembl 2021. *Nucleic Acids Res* **49**, D884–D891 (2021).
13. Kumar, S., Stecher, G., Suleski, M. & Blair Hedges, S. TimeTree: A Resource for Timelines, Timetrees, and Divergence Times. *Mol Biol Evol* **34**, (2017).
14. Tarailo-Graovac, M. & Chen, N. Using RepeatMasker to identify repetitive elements in genomic sequences. *Current Protocols in Bioinformatics* Preprint at https://doi.org/10.1002/0471250953.bi0410s25 (2009).
15. Hiller, M. *et al.* Computational methods to detect conserved non-genic elements in phylogenetically isolated genomes: Application to zebrafish. *Nucleic Acids Res* **41**, 1093 (2013).
16. Tan, G., Polychronopoulos, D. & Lenhard, B. CNER: A toolkit for exploring extreme noncoding conservation. *PLoS Comput Biol* **15**, 1–16 (2019).
17. Kent, W. J. *et al.* The Human Genome Browser at UCSC. *Genome Res* **12**, (2002).

18. Engström, P. G., Fredman, D. & Lenhard, B. Ancora: A web resource for exploring highly conserved noncoding elements and their association with developmental regulatory genes. *Genome Biol* **9**, 8–11 (2008).
19. Altschul, S. F., Gish, W., Miller, W., Myers, E. W. & Lipman, D. J. Basic local alignment search tool. *J Mol Biol* **215**, (1990).
20. Braasch, I. *et al.* The spotted gar genome illuminates vertebrate evolution and facilitates human-teleost comparisons. *Nat Genet* **48**, 427–437 (2016).
21. Katoh, K., Misawa, K., Kuma, K. I. & Miyata, T. MAFFT: A novel method for rapid multiple sequence alignment based on fast Fourier transform. *Nucleic Acids Res* **30**, 3059–3066 (2002).
22. Capella-Gutiérrez, S., Silla-Martínez, J. M. & Gabaldón, T. trimAl: A tool for automated alignment trimming in large-scale phylogenetic analyses. *Bioinformatics* **25**, 1972–1973 (2009).
23. Stamatakis, a, Ludwig, T. & Meier, H. RAxML: A Parallel Program for Phylogenetic Tree Inference. *Poster abstract in Proceedings of 2nd European Conference on Computational Biology (ECCB2003)* 325–326 (2003).
24. Darriba, D. *et al.* ModelTest-NG: A New and Scalable Tool for the Selection of DNA and Protein Evolutionary Models. *Mol Biol Evol* **37**, 291–294 (2020).
25. Rambaut, A. FigTree – Tree Figure Drawing Tool, version 1.4.3. *Molecular evolution, phylogenetics and epidemiology* (2016).
26. Rambaut, A. FigTree, a graphical viewer of phylogenetic trees. *Institute of Evolutionary Biology University of Edinburgh* (2009).
27. Emms, D. M. & Kelly, S. OrthoFinder: solving fundamental biases in whole genome comparisons dramatically improves orthogroup inference accuracy. *Genome Biol* **16**, (2015).
28. Krzywinski, M. *et al.* Circos: An information aesthetic for comparative genomics. *Genome Res* **19**, 1639–1645 (2009).
29. Hao, Z. *et al.* RIdeogram: drawing SVG graphics to visualize and map genome-wide data on the idiograms. *PeerJ Comput Sci* **6**, e251 (2020).
30. Armstrong, J. *et al.* Progressive Cactus is a multiple-genome aligner for the thousand-genome era. *Nature* **587**, 246–251 (2020).
31. Siepel, A. & Haussler, D. Phylogenetic Estimation of Context-Dependent Substitution Rates by Maximum Likelihood. *Mol Biol Evol* **21**, 468–488 (2004).
32. Pollard, K. S., Hubisz, M. J., Rosenbloom, K. R. & Siepel, A. Detection of nonneutral substitution rates on mammalian phylogenies. *Genome Res* **20**, 110–121 (2010).
33. Tang, H. *et al.* Synteny and Collinearity in Plant Genomes. *Science (1979)* **320**, 486–488 (2008).
34. Raudvere, U. *et al.* G:Profiler: A web server for functional enrichment analysis and conversions of gene lists (2019 update). *Nucleic Acids Res* **47**, W191–W198 (2019).
35. Gao, T. *et al.* EnhancerAtlas: a resource for enhancer annotation and analysis in 105 human cell/tissue types. *Bioinformatics* **32**, 3543–3551 (2016).
36. Polychronopoulos, D., King, J. W. D., Nash, A. J., Tan, G. & Lenhard, B. Conserved non-coding elements: Developmental gene regulation meets genome organization. *Nucleic Acids Res* **45**, 12611–12624 (2017).
37. Kikuta, H. *et al.* Genomic regulatory blocks encompass multiple neighboring genes and maintain conserved synteny in vertebrates. *Genome Res* **17**, 545–555 (2007).

38. Chiang, C. W. K. *et al.* Ultraconserved Elements: Analyses of Dosage Sensitivity, Motifs and Boundaries. *Genetics* **180**, 2277–2293 (2008).
39. Walter, K., Abnizova, I., Elgar, G. & Gilks, W. R. Striking nucleotide frequency pattern at the borders of highly conserved vertebrate non-coding sequences. *Trends in Genetics* **21**, 436–440 (2005).
40. McEwen, G. K. *et al.* Early evolution of conserved regulatory sequences associated with development in vertebrates. *PLoS Genet* **5**, (2009).
41. Woolfe, A. *et al.* Highly conserved non-coding sequences are associated with vertebrate development. *PLoS Biol* **3**, (2005).
42. Takahashi, M. & Saitou, N. Identification and characterization of lineage-specific highly conserved noncoding sequences in mammalian genomes. *Genome Biol Evol* **4**, 641–657 (2012).
43. Babarinde, I. A. & Saitou, N. Heterogeneous tempo and mode of conserved noncoding sequence evolution among four mammalian orders. *Genome Biol Evol* **5**, 2330–2343 (2013).
44. Lowe, C. B. *et al.* Three periods of regulatory innovation during vertebrate evolution. *Science (1979)* **333**, 1019–1024 (2011).

FIGURES

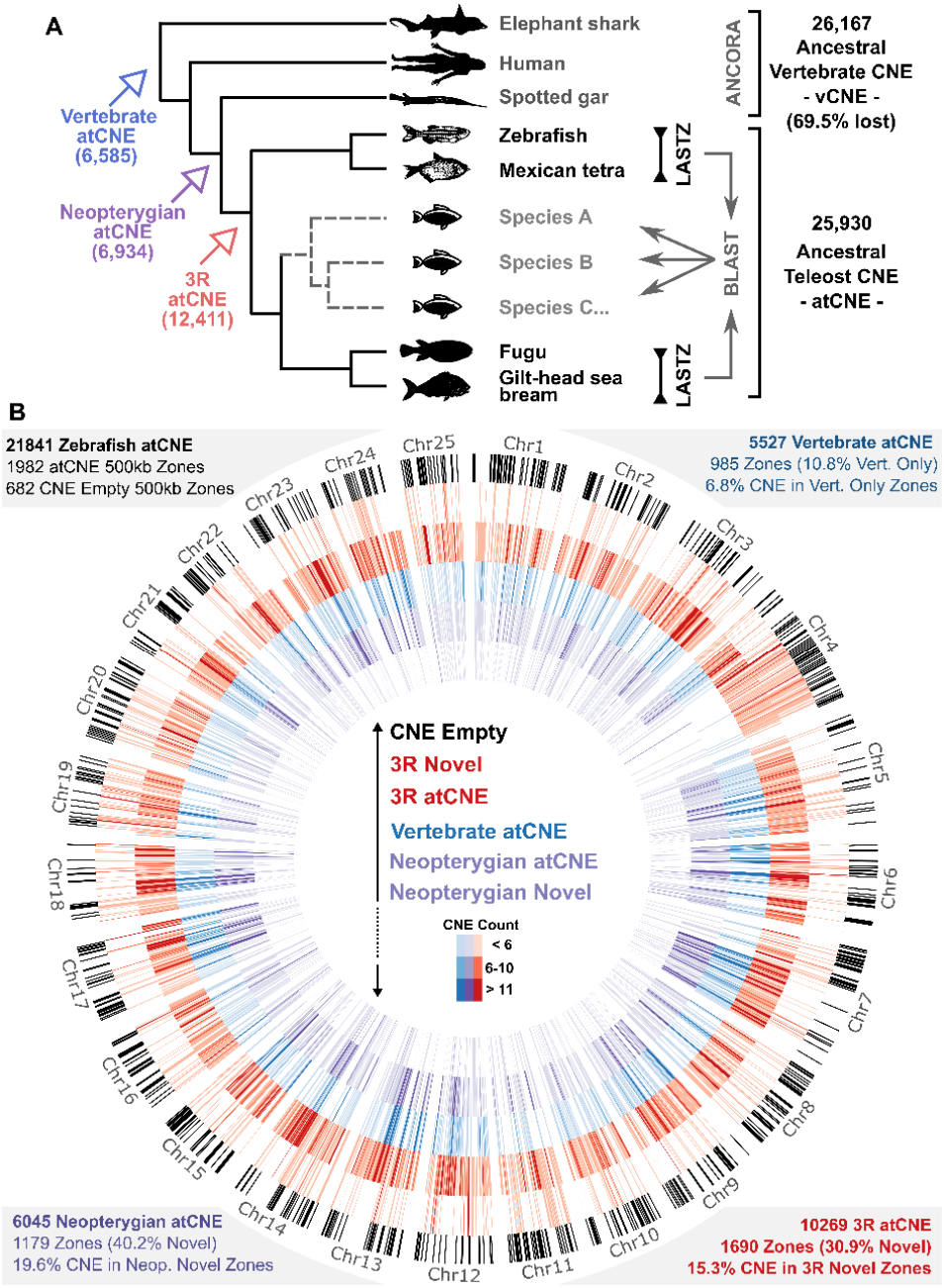

Figure 1. Teleost ancestral CNE identification and distribution. A. CNE sets from pairwise whole genome alignments in two focal reference genome pairs (LASTZ) were searched in 20 other

teleost genomes via BLAST, identifying 25,930 atCNEs that were present in the teleost common ancestor. Comparison to non-teleost vertebrate genomes and ancestral vertebrate CNEs from the ANCORA database revealed widespread loss of vertebrate atCNEs and gain of novel atCNEs in Neopterygians and Teleosts(3R). **B.** Distribution and count of 21,841 atCNEs over 1,982 500kb-long zones in the zebrafish genome. From largest (outermost) to smallest (innermost) circle radius: 1) Genomic regions with no atCNE presence (black). 2) Novel zones with 3R atCNE presence (red) and absence of older (neopterygian or vertebrate) atCNE. 3) Zones with 3R atCNE presence (red). 4) Zones with vertebrate CNE presence (blue). 5) Zones with Neopterygian atCNE presence (purple). 6) Novel zones with Neopterygian atCNE presence (purple) and absence of older (Vertebrate) atCNE.

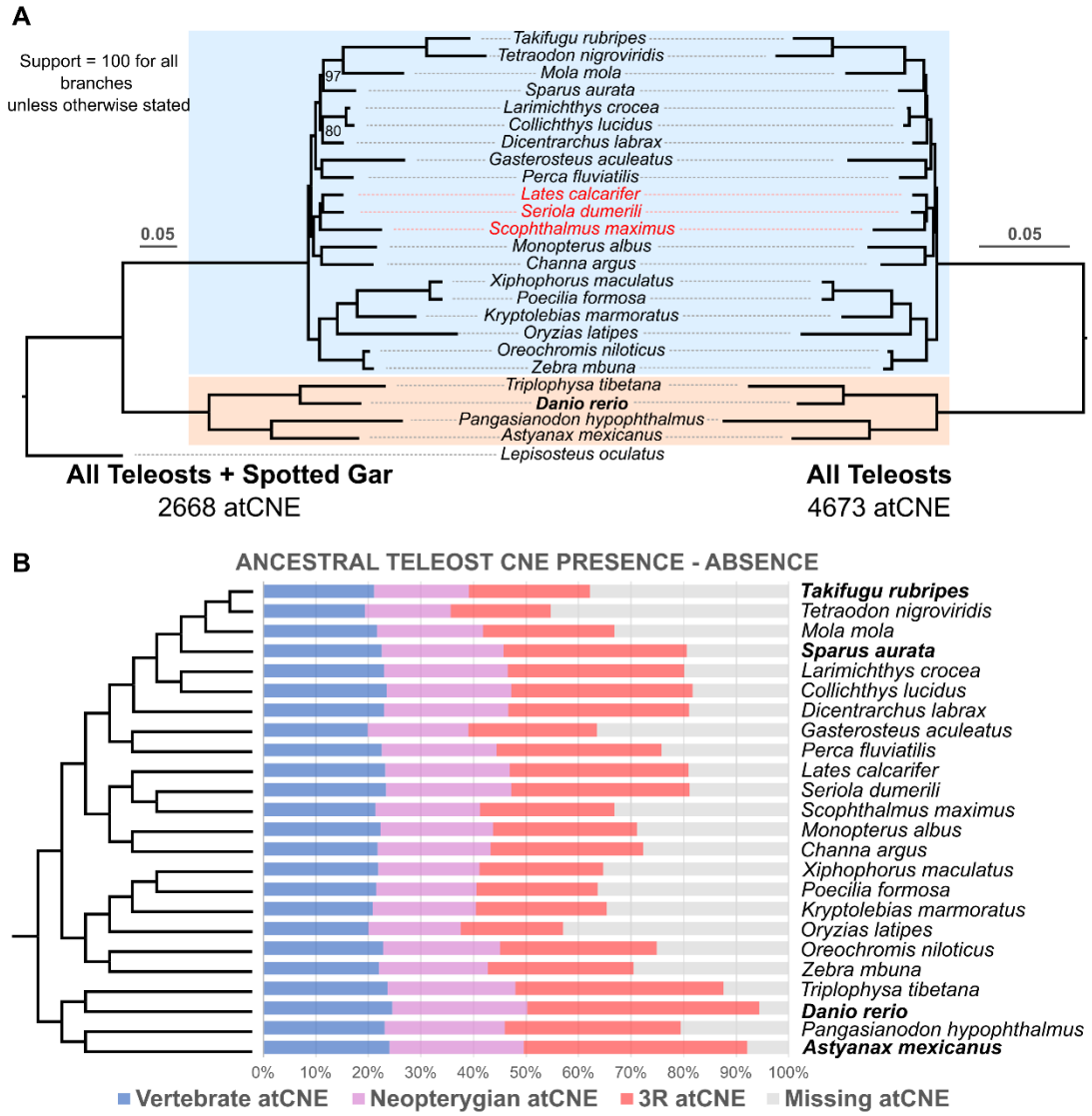

Figure 2. Ancestral CNE losses across the teleost phylogeny. A. Phylogenetic reconstruction of the relationships of the 24 teleost species included in the study, using single copy universal atCNEs, including (left tree – 2668 atCNEs) or excluding (right tree – 4673 atCNEs) spotted gar. The two basally diverged clades used to infer ancestral teleost CNEs are highlighted with orange (clade 1) and blue (clade 2). **B.** Presence / absence of ancestral atCNEs of different origin categories

(Vertebrate in blue, Neopterygian in purple, 3R in red) in different species in our phylogeny as a percentage of total identified atCNEs. The cladogram is constructed based on our phylogenetic reconstructions.

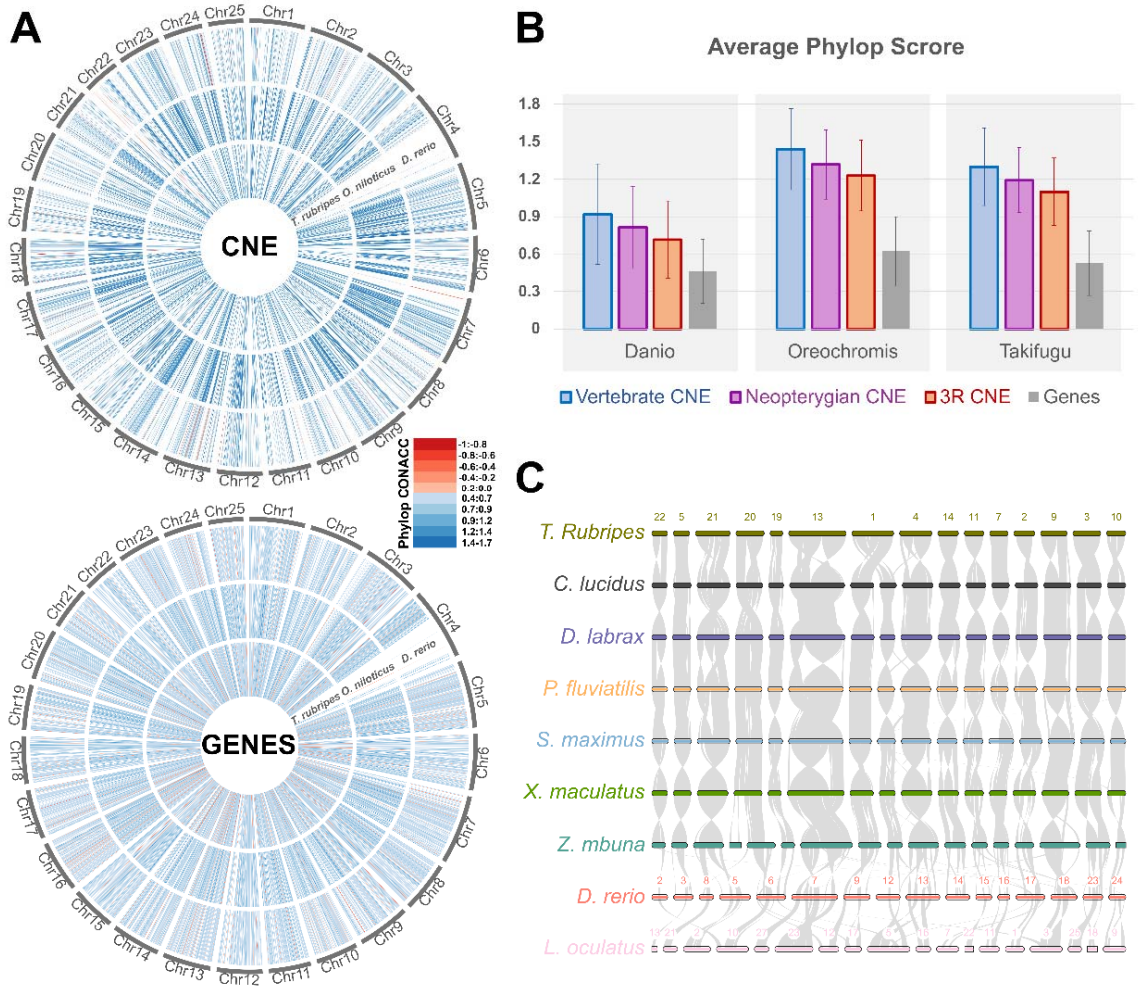

Figure 3. CNE sequence and synteny conservation. A. PhyloP (CONACC) Conservation scores for atCNEs and Genes in *D. rerio*, *O. niloticus* and *T. rubripes* mapped on *D. rerio* chromosomes. **B.** Average phyloP (CONACC) conservation scores and standard deviation for atCNEs in different categories and genes in *D. rerio*, *O. niloticus* and *T. rubripes*. **C.** Synteny of atCNEs across 8 teleost genomes and *L. oculatus*.

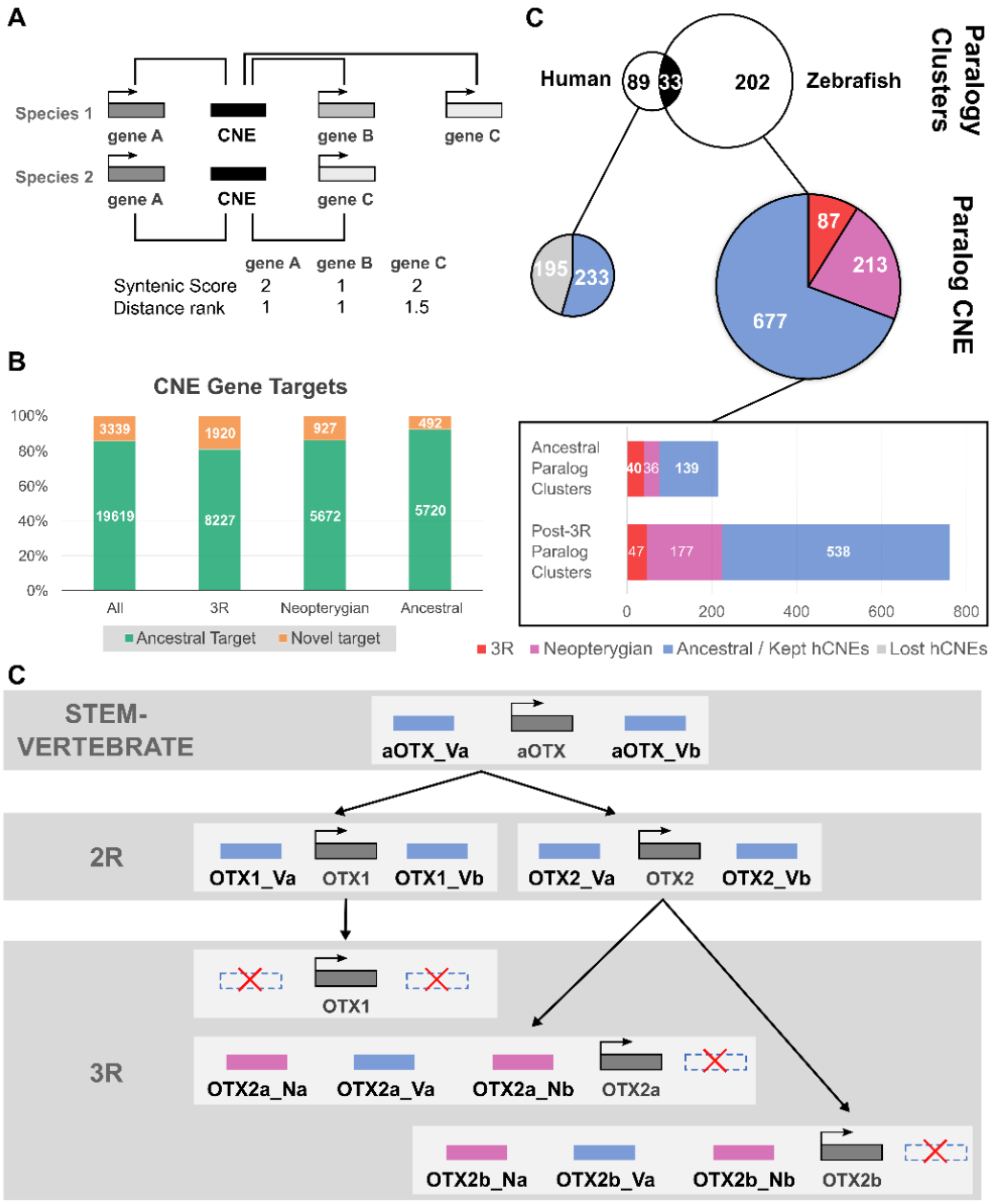

Figure 4. CNE-gene target association and paralog analysis. **A.** CNE were linked to putative target genes though orthology-guided synteny-based association, using the maximal syntenic score (number of species a CNE-gene pair is found within 1Mb) and minimal proximity rank (position of a gene to a CNE when all genes are ordered in increasing distance) for each CNE-target pair. **B.** Percentage (and counts within boxes) of ancestral (avCNE also proximal to orthologous locus in human) or novel gene targets for atCNEs in different categories. **C.** Paralogy cluster and paralog CNE counts for different categories in human / other vertebrates (left) or zebrafish / teleosts (right). Common paralogy clusters between the two groups are shared in black and common / ancestral atCNEs within paralogy clsuters are shown in blue. **D.** CNE gains, duplications and losses in the *OTX1* / *OTX2* paralogous loci in vertebrates and teleosts.

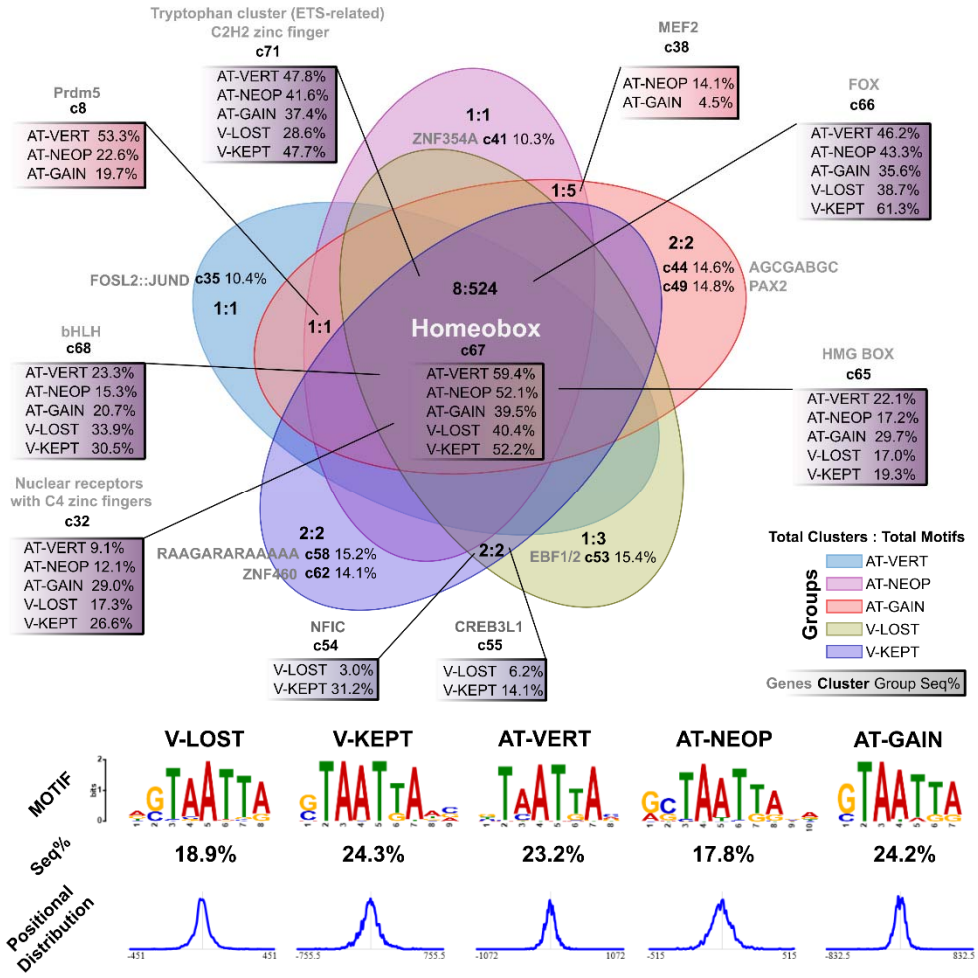

Figure 5. Motif Discovery and Transcription Factor Binding Site Enrichment. **TOP**. Overlap of enriched TFBS categories among combinations of atCNEs (AT-VERT : Vertebate - Blue, AT-NEOP Neopterygian - Purple, AT-GAIN : 3R - Red) and avCNEs (V-KEPT : Kept in Teleosts - Dark Purple, V-LOST : Lost in Teleosts - Yellow). Enrichment overlaps are displayed in the format "Total Categories: Total Enriched Motifs" in each overlap area. The percentage of sequences of each CNE group with motifs in representative categories (c1, c2…) are shown. **BOTTOM.** Percentage of sequences in each CNE group that contain the most common shared de-novo predicted motif (consensus TAATTA) and its positional distribution.

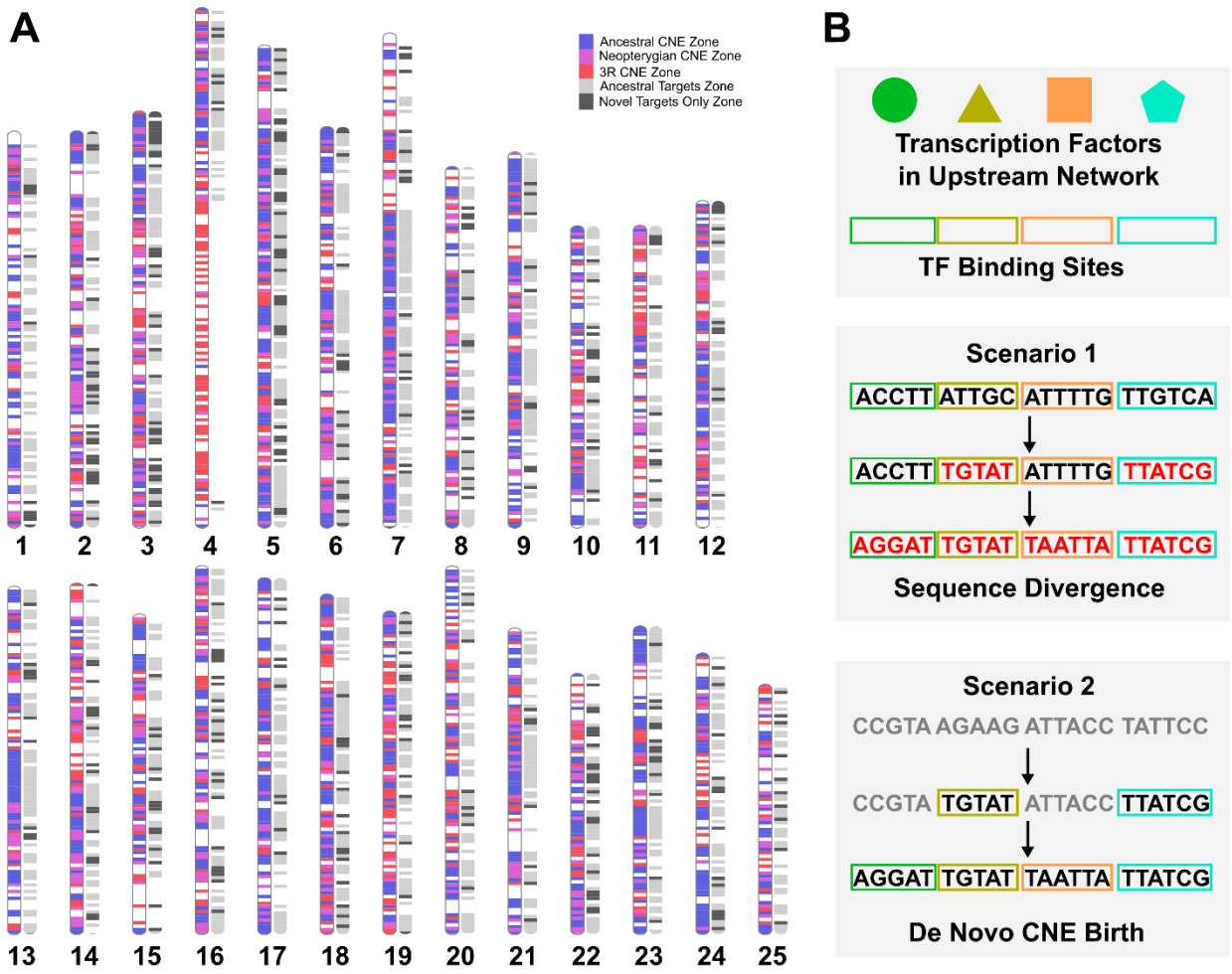

Figure 6. **Teleost CNE-target localization and models of CNE gain. A.** Localization of atCNEs and associated target genes in zebrafish chromosomes. CNE zones are plotted in blue if they contain vertebrate atCNEs, in purple if they contain neopterygian atCNEs and do not contain vertebrate atCNEs, in red if they contain 3R atCNEs and do not contai any older (vertebrate or neopterygian) atCNEs. Gene zones are plotted in light grey if they contain ancestral targets or in dark grey if they contain only novel targets and do not contain ancestral targets. **B.** Two hypothesized scenarios of atCNE gain: Scenario 1) Extreme sequence divergence of ancestral sequence renders CNE unrecognizable, while TFBS are preserved. Scenario 2) CNE gain through de novo emergence.

Table 1. Gene Ontology Enrichment for ancestral and novel CNE gene target sets.

term_id	term_name	Padj Ancestral Target	Padj Novel Target	Ansetral Target Examples	Novel Target Examples
GO:0032502	developmental process	7.14E-48	1.60E-09	shox2,twist3,meis2a,smad1,tlx1	nectin1b,pbx4,foxo6b,elf1,gli1
GO:0007399	nervous system development	9.48E-39	1.69E-02	pbx3b,wnt3,foxd3,irx2a,pax6b	neurod4,fgf24,notch3,irx7,meis3
GO:0030154	cell differentiation	1.22E-28	3.64E-07	gata6,smad6b,nr2f2,prdm8b,fgf4	smad4a,foxd2,myog,wnt6b,nkx3.3
GO:0022008	neurogenesis	4.75E-26	5.56E-03	LHX3,neurod2,prox1a,fgf19,irx1a	wnt11,ntrk1,sema4c,sox10,anxa1a
GO:0007166	cell surface receptor signaling pathway	3.24E-06	1.32E-02	lef1,wnt8b,fgf20b,her6,DTX1	pappa2,sema3fa,stat6,nod2,fgf22
GO:0007267	cell-cell signaling	1.05E-05	4.89E-03	gbx1,axin2,panx3,nkx6.1,cacna1ba	lbx2,wnt8a,tet3,GRM7,cacng8b
GO:0007169	transmembrane receptor protein tyrosine kinase signaling pathway	1.82E-04	2.41E-02	zeb2a,ERBB4,fgfr2,ntrk2b,nrg1	efna3a,ltk,fgfrl1a,ntrk1,fgf22
GO:0010468	regulation of gene expression	1.29E-23		dmbx1a,foxf2a,tbx2b,barx2,gsx1	
GO:0060429	epithelium development	1.07E-12		tbx21,glis2b,runx2b,tfap2c,gata5	
GO:0007167	enzyme-linked receptor protein signaling pathway	7.12E-09		ntrk2b,pappaa,fgf10a,tgfb3,dusp6	
GO:0070848	response to growth factor	6.95E-08		fgfr2,tgfbr3,smad7,vegfc,fgf1b	
GO:0003002	regionalization	1.64E-07		bmb2b,dmrt2a,tcf7,sox17,vent	
GO:0007423	sensory organ development	3.34E-07		pbx1a,irx2a,six3a,meis1b,hmx1	
GO:0035295	tube development	9.20E-07		fgf10a,twist1a,sox7,onecut1,meis1b	
GO:0030900	forebrain development	9.67E-06		prox1a,eya1,pax6b,gli2a,nkx2.1	
GO:0072359	circulatory system development	9.79E-06		smarca5,unc5b,mef2aa,twist1a,foxc1a	
GO:0007507	heart development	1.10E-04		enc3,fxr1,pou4f1,tbx19,dkk1b	
GO:0048839	inner ear development	1.16E-04		pax2a,hmx2,eya2,bmp2b,esrrga	
GO:0048732	gland development	2.00E-04		rpl3,dhpsnr5a2,xbp1,met,prickle1a	
GO:0001501	skeletal system development	8.87E-04		col1a2,faf1,bcl9,egf,ostn	
GO:0045055	regulated exocytosis		4.18E-02		otofa,SYT2,cacna1g,rims3,unc13ba

Supplementary Data

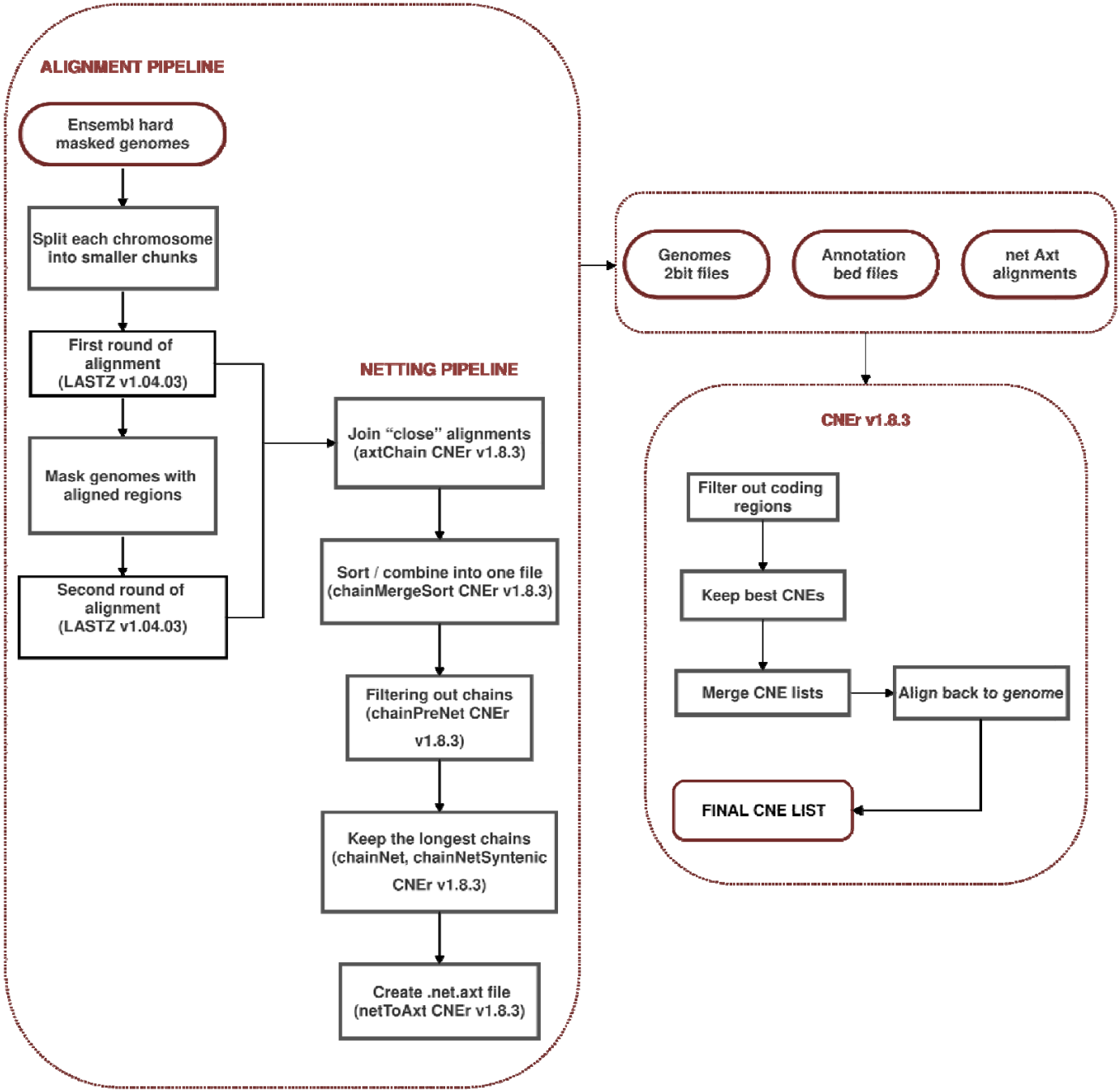

Supplementary Figure 1. Alignment pipeline. Two rounds of pairwise whole-genome alignments using masked genomes. **Netting pipeline**. Join close alignments and form chains, then select the longest chains. **CNEr v1.8.3.** CNE Identification pipeline using genomes in 2bit format, annotation

bed files and the chained alignments as input. The output of this pipeline is a list with all identified CNEs.

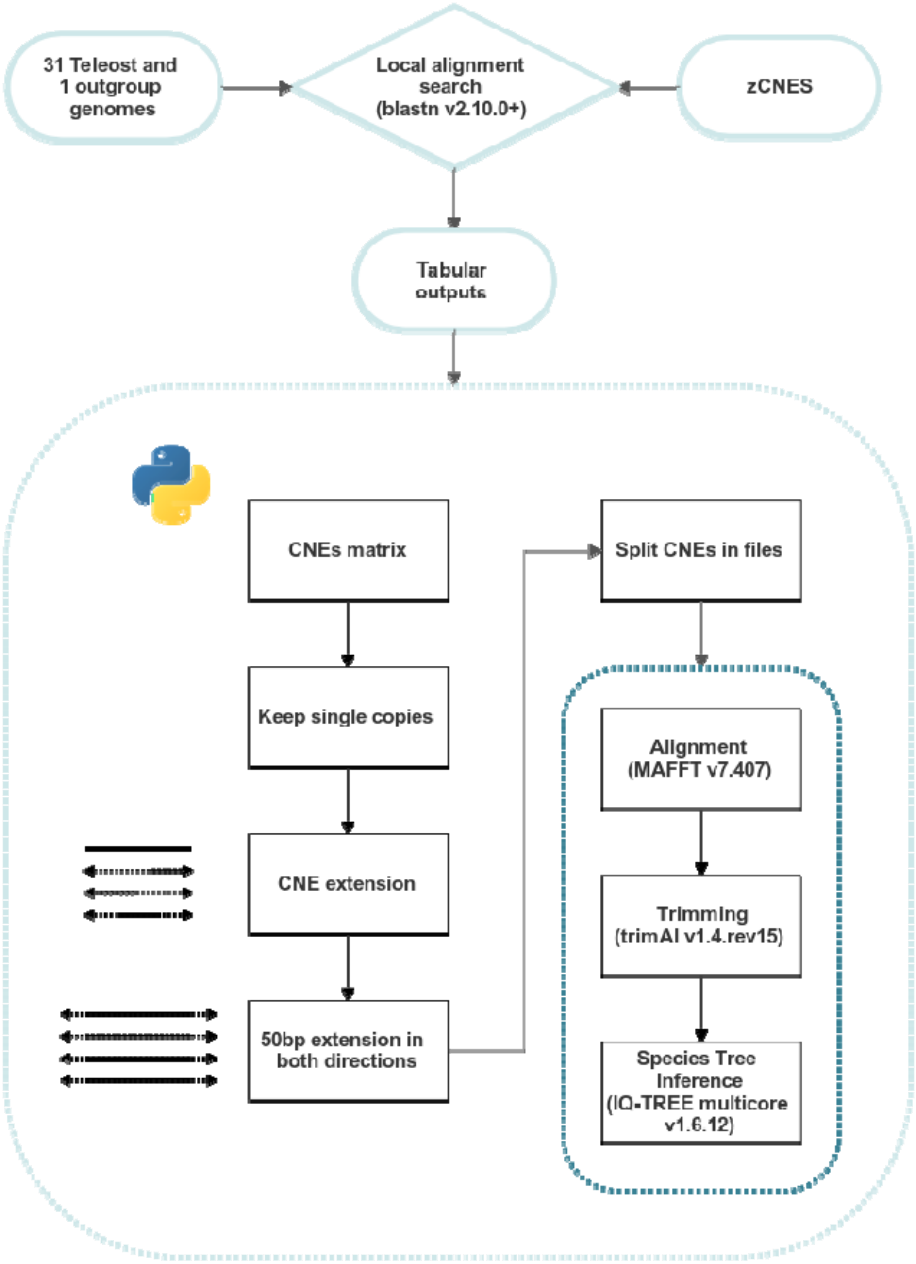

Supplementary Figure 2. CNE processing pipeline and CNE-based tree construction using single copy CNE orthologs.

Supplementary Table 1. BLAST results

Species	# of zCNEs	# of fCNEs	# of hCNEs
A. mexicanus	57551	4532	5350
C. argus	16455	26226	4562
C. lucidus	18029	32927	4768
D. rerio	63023	5074	4932
D. labrax	18471	33585	5340
G. aculeatus	14497	23361	4420
K. marmoratus	14563	21202	4667
L. crocea	18187	32965	5321
L. calcarifer	18420	32046	5410
M. mola	14729	30942	4700
M. albus	15834	26227	4995
O. niloticus	16856	27584	5075
O. latipes	12454	16772	4275
P. hypophthalmus	40328	4625	4508
P. fluviatilis	16727	32237	4884
P. formosa	13910	19958	4535
S. maximus	14241	27135	4498
S. dumerili	18296	32193	5362
S. aurata	18476	37371	5202
T. rubripes	12526	39532	4329
T. nigroviridis	11469	32867	3955
T. tibetana	55660	4967	4789
X. maculatus	13764	19640	4554
Z. mbuna	15297	27592	4672